HALF-WIDTH SCALING OF ELECTRIC FIELD AUTOCORRELATION FUNCTIONS OF LIGHT SCATTERED FROM BULL SPERMATOZOA

T. CRAIG AND F. R. HALLETT
Department of Physics, University of Guelph, Guelph, Ontario N1G 2W1, Canada

ABSTRACT The half-width scaling of experimental and model electric field autocorrelation functions of light scattered from normally swimming, defectively swimming, and immotile bull spermatozoa is examined. It is found that a scatterer of size 9.0 × 2.3 × 0.45 μm is most appropriate for this Rayleigh-Gans-Debye ellipsoid model. In the case of the immotile cells, this model correctly predicts the features seen in the scaling data as well as the absolute value of the data. For the normally swimming and defective populations the model proves to predict correctly the features seen in the experimental scaling curves, but not the absolute value of the data. This discrepancy appears to be related to a lack of detail in the model, since the agreement is poorest at large scattering angles.

INTRODUCTION

The agreement between the values and shapes of half-widths of experimental and model autocorrelation functions at different scattering angles has been taken to be the ultimate test of a model. It has been used in the case of *Escherichia coli* by Holz and Chen (1978*a* and *b*) to show that their model was at least qualitatively correct, and it helped them to distinguish between a straight-line motion model and a helical motion model. They also postulate, correctly, that the nonscaling behavior that they observe will survive an averaging over a frequency distribution for this motion. They do not do this averaging. Their model was a model of the Rayleigh-Gans-Debye (RGD) type.

In a later paper by Kotlarchyk et al. (1979), the effect of this RGD approximation on the scattering amplitudes and correlation functions was investigated. Here the RGD approximation was compared with the extended Mie theory of Asano and Yamamoto (1975). It was found that as long as the relative index of refraction of the particle was small the discrepancies between the RGD and Mie theories were negligible, especially at low scattering angle. These differences could certainly never be distinguished in the data.

Ascoli et al. (1978) have also used scaling to show that their model for the swimming of *Euglena* is correct. Their measurements were done in the frequency domain, and the Doppler shifts they predicted at different scattering angles were very close to those seen.

A recent study by Racey et al. (1981) has shown that the point particle model is a good one for the autocorrelation functions from *Chlamydomonas reinhardtii*. They do this by noting that the experimental autocorrelation functions scale as the inverse of the scattering vector $\mathbf{k}$, whose magnitude is related to the scattering angle θ through $k = (4\pi n/\lambda)\sin(\theta/2)$. This result is consistent with expectations based on the point particle model.

One previous study exists for the scaling properties of light scattered from spermatozoa. This is a quasi-electric light-scattering study of the spermatozoa of the abalone and pig by Shimizu and Matsumoto (1977), who claimed that their autocorrelation functions when plotted as a function of $k\tau$ did not depend on scattering angle, which lead them to believe that the point particle model was correct and that orientational and rotational effects are negligible. Their angular resolution, however, was not good enough to support this claim.

In this paper we shall present data showing that orientational effects and cellular shape strongly affect the scaling behavior of the bull spermatozoan system.

THEORY

The bull spermatozoon cell is made up of an ellipsoidal head of semiaxes 4.5 × 2.3 × 0.5 μm, a roughly cylindrical midpiece region of radius 0.5 μm and length 15 μm, and finally a thin tail of length 35 μm. Since most samples of bull spermatozoa contain three populations of scatterers—the normal or helically swimming cells, the defective or circularly swimming cells, and the immotile (diffusing or sinking) particles—the correlation functions must be split into the three component functions, which are modeled as follows.

Normally Swimming Spermatozoa

The normally swimming cells swim in a helical path with a pitch of ~12 μm and a radius of ~3.2 μm. Their linear speed along the axis of this helix is ~110 μm/s and the frequency around the helix is ~10 Hz. Since most of the light scattered by a sperm cell is scattered by the head (Rikmenspoel, 1964), the first model chosen by Craig et al. (1979) to represent this cell was one of an ellipsoid moving along a helix. It was found that an equivalent ellipse of semiaxes 9.0 × 2.3 × 0.5 μm was needed to generate

functions that matched the data. This increased length of the long axis of the head over its physical value is believed to be due to the fact that the midpiece of the cell also contributes to the scattered intensity.

Using this model and including the dynamic properties of the cell, Craig et al. (1979) determined that the model correlation function needed to fit the data has the form

$$g^{(1)}(\tau) = C_N^{-1} R \int_0^1 d\nu \sum_n (1 + iq_\nu)^{-2} (1 + ip_n)^{-2} |B_n|^2, \quad (1)$$

where C_N^{-1} is a normalization constant; R denotes the real part of the expression; $\nu = \cos\theta$, where θ is the angle between the scattering vector $\mathbf{k}$ and the direction of motion; and

$$q_\nu = \frac{1}{2} k\bar{v}\tau, \quad (2)$$

$$p_n = \frac{1}{2} n\bar{\omega}\nu\tau. \quad (3)$$

and the B_n are related to the dynamic form factor, $A(\mathbf{k}, \tau)$. In these expressions, $\bar{v}$ is the average speed, $\bar{\omega}$ the average angular frequency, τ the experimental delay time, and ψ the instantaneous phase of the particle on its helical path; i.e., the helical motion is described by

$$\psi = \psi_0 + \omega\tau. \quad (4)$$

Eq. 1 is obtained by using distributions of speed and angular frequency:

$$P_s(v) \sim v e^{-2v/\bar{v}} \quad (5)$$

and

$$P(\omega) \sim \omega e^{-2\omega/\bar{\omega}}. \quad (6)$$

A coat was also added by using the method of Chen et al. (1977), which served to alter the set of B_n used.

Defectively Swimming Spermatozoa

Although the defectively swimming cells have structural properties that appear identical to normal cells, they have a completely different trajectory. The overall path of their motion is a circle, with the head oscillating back and forth across the circular track. The largest of the two small axes of the cell is in the plane of the circle. The speed of this motion is ~90 μm/s, with an oscillatory frequency of ~15 Hz.

The model of Craig et al. (1982) will be used for the scaling work presented here. The form of the autocorrelation function was determined to be

$$g^{(1)}(\tau) = C_N^{-1} \int_0^1 d\nu \int_0^\pi d\psi \sum_n \cos(n\bar{\omega}\tau) \cos(k\bar{v}\nu\tau) e^{-n^2\tau^2\sigma_\omega^2/2} e^{-k^2\nu^2\tau^2\sigma_v^2/2} |B_n|^2 \quad (7)$$

The variables in Eq. 7 are similar to those in Eq. 1, except that the variance of the average speed σ_v and the variance of the average frequency σ_ω are now included. These arise from the distributions

$$P_s(v) \sim e^{-(v-\bar{v})2/2\sigma_v^2}, \quad (8)$$

$$P(\omega) \sim e^{-(\omega-\bar{\omega})^2/2\sigma_\omega^2}, \quad (9)$$

which gave best agreement with cinematographic data and best fit to correlation functions obtained at low angle (Craig et al., 1982). A more complete description of the origin of Eq. 7 appears in Craig et al. (1982).

A coat representing the outer layers of the cell was added to the ellipsoid according to methods described by Chen et al. (1977).

Immotile Cells

The immotile fraction of the samples was found to contain a diffusive portion consisting of fat globules and other cellular debris and a sedimenting portion made up of bull sperm cells rotating slowly as they sink (Fig. 1). The corresponding correlation function is

$$g^{(1)}(\tau) = \alpha e^{-Dk^2\tau} + (1 - \alpha) F_N(\tau), \quad (10)$$

where D represents the average diffusion coefficient of the debris and F_N represents the scattering function of the sedimenting sperm cells. The general form of the correlation function for a translating, rotating, nonpoint particle is (Craig et al., 1979)

$$g^{(1)}(\tau) = C_N^{-1} \left\langle R \int_0^1 d\nu\, e^{ik\nu\nu\tau} \sum_n |B_n|^2 e^{in\omega\tau} \right\rangle, \quad (11)$$

where all the parameters are as specified earlier, and the angle braces indicate averaging over dynamic quantities. It is necessary to specify a $P_s(v)$ and $P(\omega)$ to evaluate the averages in Eq. 11. However, in the case of a cell sinking through the scattering volume the direction of motion is perpendicular to the scattering vector, so that $\nu = \cos\theta = 0$. This yields $F_N(\tau)$, which is given as

$$F_N(\tau) = C_N^{-1} \left\langle R \sum_n |B_n|^2 e^{in\omega\tau} \right\rangle. \quad (12)$$

It is now necessary only to specify a $P(\omega)$ to evaluate Eq. 12. The $P(\omega)$ chosen for this study was

$$P(\omega) \sim \omega^2 e^{-3\omega^2/2\bar{\omega}^2}, \quad (13)$$

as was chosen by Holz and Chen (1978*a*) for motile *E. coli*. This distribution was chosen since it resembles a shifted normal distribution, but it does not contain a width parameter σ_ω^2, as does Eq. 9. Eq. 12 then becomes

$$F_N(\tau) = C_N^{-1} \sum_n e^{-\Delta^2/4} \left(1 - \frac{\Delta^2}{2}\right) |B_n|^2, \quad (14)$$

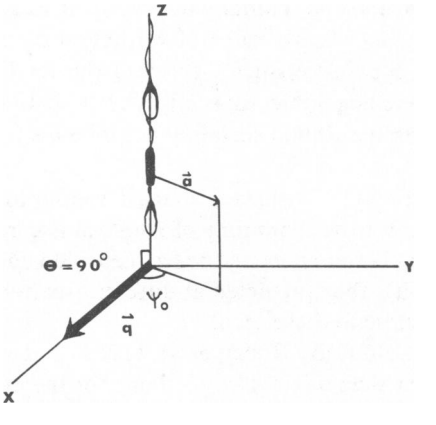

FIGURE 1 Orientation of the sinking rotating immotile bull spermatozoon in the scattering geometry.

where

$$\Delta = n\bar{\omega}\tau\sqrt{\frac{2}{3(0.846)}}. \qquad (15)$$

Only positive values of n and the $n = 0$ term need be considered in Eq. 14, since it is even in nature. Including Eq. 14 in Eq. 10 yields a final form of the autocorrelation function of the immotile fraction:

$$g^{(1)}(\tau) = \alpha e^{-Dk^2\tau} + (1-\alpha)C_N^{-1}\sum_n e^{-\Delta^2/4}\left(1-\frac{\Delta^2}{4}\right)|B_n|^2. \qquad (16)$$

A coat was sometimes included in the calculations of the $F_N(\tau)$ functions as well.

Experimental Methods

The general light-scattering arrangement has been described before (Hallett et al., 1978). All autocorrelation functions taken at a scattering angle of 15° were done on this apparatus at a temperature of 30 ± 0.5°C. The functions taken at other scattering angles were determined with the circular scattering cell shown in Fig. 2, which also was controlled to 30° ± 0.5°C. The two essential features of this cell are the light trap opposite the entrance port for the light and the light-absorbing material on the opposite wall of the glass sample holder from the photomultiplier. Both features serve to stop reflected light from entering into the photomultiplier when it is in a back-scatter geometry. This reflected light would serve to give anomalously high values for the half-width. This cell was calibrated with 0.255-μm latex spheres (Duke Scientific Corp., Palo Alto, CA). The diffusion coefficient for these spheres was found to be correct and constant over all the scattering angles used in this investigation.

Most details regarding the handling and dilution of the semen samples has been described before (Hallett et al., 1978; Craig et al., 1979, 1982), as have the numerical methods (Craig et al., 1979, 1982). In the present study, it was necessary to obtain many autocorrelation functions from a particular segment of the spermatozoan population (e.g., the normal swimmers) over a range of scattering angles. This led to several complications, since the sperm gradually slow down and die over the duration of the experiment. Because of this, the immotile portion had to be subtracted from the autocorrelation function at any particular angle and the width of the resulting autocorrelation function normalized to $t = 0$ in order to compare functions taken at different times and angles.

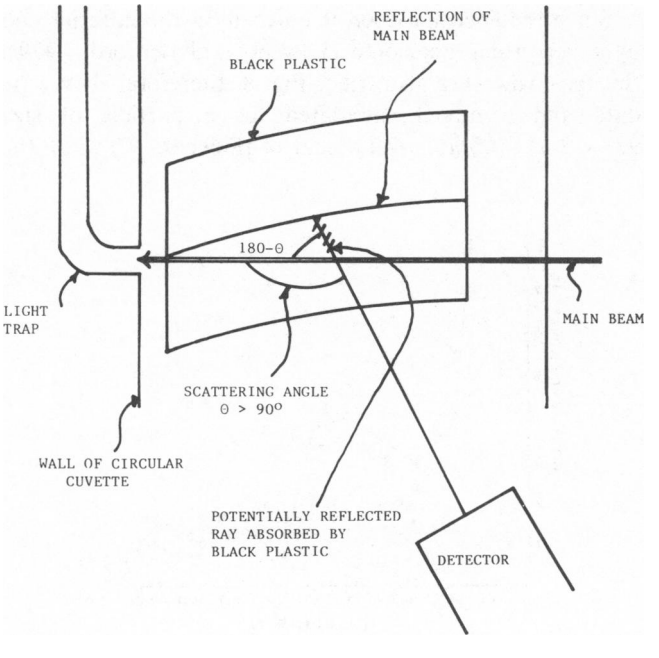

FIGURE 2 Round scattering cell used for taking autocorrelation functions at angles >15°. The positions of the light trap and the nonreflecting black plastic are shown.

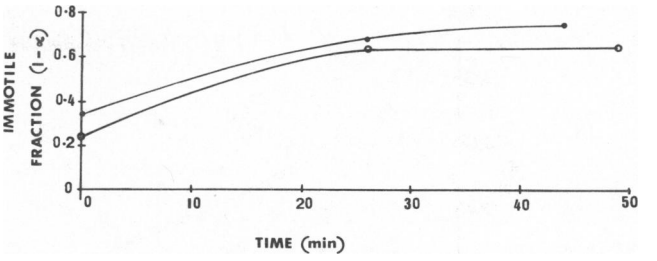

FIGURE 3 Two examples of plots of the fractions of immotile cells in samples of only normally swimming and immotile cells as a function of time, as determined by light scattering.

The following procedures were followed for both normal and defective populations. We shall use the normal cells as an example, however. Samples were chosen with only immotile and normally swimming cells. This was checked microscopically and any samples deviating from this were discarded. Experiments were performed at a scattering angle of 15°, at two other scattering angles (θ_1 and θ_2), and then at 15° again. This pattern was continued until there were not enough live cells remaining. This occurred when the live cell fraction fell below 20%. The autocorrelation functions at 15° were fit according to the method of Hallett et al. (1978) to obtain the fraction of dead cells and the half-width of the normal population. This method does not use the immotile function derived in Eq. 16. However, over the time scales of the correlation functions for both the normal and defective cells both of these immotile functions appear as flat lines. These values were then plotted as a function of time as shown in Fig. 3 and 4, respectively. Then the fraction of dead cells at θ_1 was deduced by interpolating between the points plotted in Fig. 3.

An aliquot of the original sample was allowed to die in the refrigerator (0.5 mg/ml streptomycin sulfate was added to this aliquot to stop bacterial growth). Autocorrelation functions at various scattering angles (θ) were determined for this sample. The resulting functions were subtracted from the data obtained at θ_1 and all other scattering angles obtained from that particular sample. The remaining function corre-

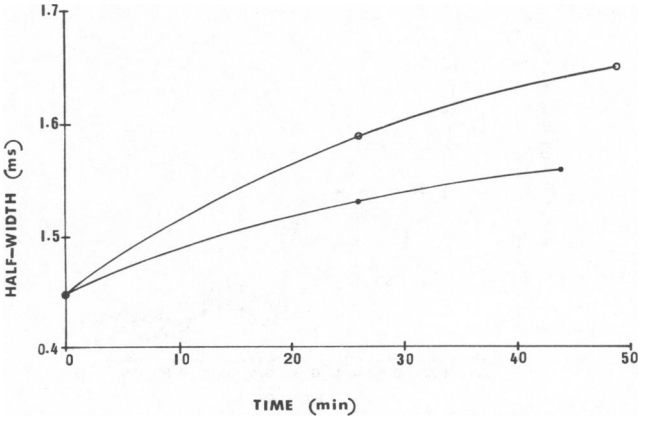

FIGURE 4 Two examples of plots of the half-widths of autocorrelation functions from normally swimming cells as a function of time.

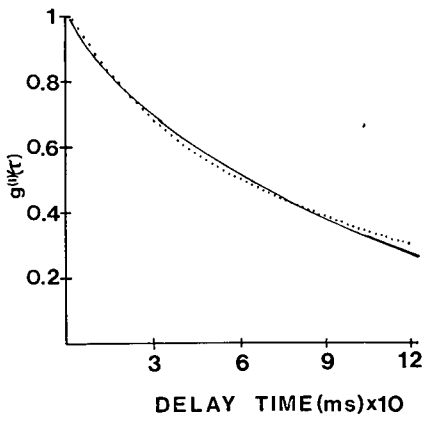

FIGURE 5 Experimental autocorrelation function (· · ·) from an immotile sample at a scattering angle of 15° and a fit generated with Eq. 16 (—). The model ellipsoid had semiaxes 9.0 μm × 2.3 μm × 0.5 μm. α = 0.35, D = 5.5 × 10^{-12} m^2/s, and $\bar{f}$ = 0.69 Hz. Different samples yielded values of $\bar{f}$ ranging from 0.30 Hz to 0.70 Hz.

sponds to the scattering function of the normal cell population with half-width ($Hw_{\theta_1, t-t'}$). The normalized half-width ($Hw_{\theta_1, t-0}$) of the function was determined by interpolating between the points on Fig. 4. $Hw_{15°, t-t'}$ and the normalized half-width values were related as follows:

$$Hw_{\theta_1, t-0} = Hw_{\theta_1, t-t'} (Hw_{15°, t-0}/Hw_{15°, t-t'}). \quad (17)$$

A similar procedure was followed also for the circularly swimming cells. The experimental scaling curves shown later are the results of doing at least five such determinations at each scattering angle.

RESULTS

Immotile Cells

The results from immotile samples are presented first because these samples were stable for long periods of time and gave us the best quality functions against which our model could be tested. A typical fit to the data at a scattering angle of 15° from the immotile cells using Eq. 16 is shown in Fig. 5. The scatterer was chosen to have the standard size of 9.0 × 2.3 × 0.5 μm. At first, no coat was added. The best fit occurred when α = 0.35, D = 5.5 × 10^{-12} m^2/s, and $\bar{f}$ = 0.69 Hz. The values of α and D indicate that ~35% of the scattered light arises from cellular and other debris having an average size of ~4.0 × 10^{-2} μm. The small size justifies our not including an additional time-dependent prefactor in the diffusive term of Eq. 16, since this radius is small compared with the wavelength of the light used. The addition of a coat had essentially no effect on the fit or the curve shape shown in Fig. 5.

The scaling behavior of Eq. 16 is now examined. This is shown in Fig. 6 for a particle having the standard shape with α = 0.35, D = 5.5 × 10^{-12} m^2/s, and $\bar{f}$ = 0.38 Hz. Also shown in this figure are the experimental half-widths from immotile samples. The vertical line at each data point indicates the standard error of the mean of the average value shown. Remarkable agreement between the features in the two curves is seen, although the peaks in the two curves are slightly out of register. Small changes in the b or c axis made negligible changes in the scaling behavior of the model functions. Changing a, however, had a marked effect on the positions of the peaks. Making this semiaxis smaller tends to move the peaks out to higher **k**, whereas making it larger tends to move them in. The optimum a value remained at 0.5 μm. The curve in Fig. 7 is one generated with the standard particle but with the addition of a coat of thickness 0.01 μm and index of refraction 1.42. The interior index of refraction was taken to be 1.35 (van Duijn and van Voorst, 1971). The addition of this thin coat did not change the agreement between the data and model appreciably, although the peaks were shifted slightly to lower values of **k**.

Since the spermatozoon is covered on the anterior end by a very thick acrosome (Fawcett and Bedford, 1979), thicker coats were also tried. Fig. 8, therefore, shows the data and a model calculated for a particle of size 9.0 × 2.3 × 0.5 μm with a coat of thickness 0.27 μm, the

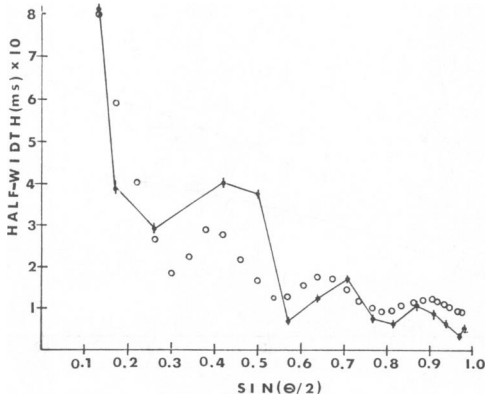

FIGURE 6 Scaling curve for the data from immotile cells (●) and points calculated with Eq. 16 (○) for the uncoated standard-shaped particle with α = 0.35, D = 5.5 × 10^{-12} m^2/s, and $\bar{f}$ = 0.38 Hz.

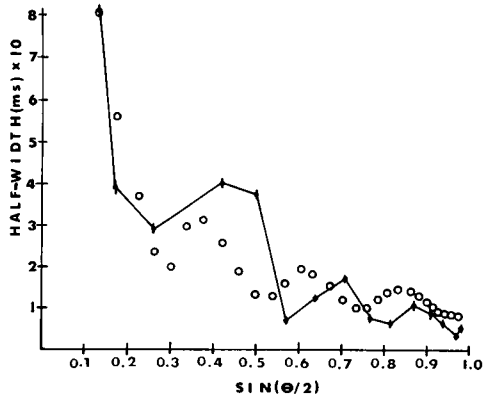

FIGURE 7 Scaling curve for the data from immotile cells (●) and points calculated with Eq. 16 (○) for the standard shaped particle with a coat of thickness 0.01 μm and index of refraction of 1.42. The interior index of refraction is 1.35.

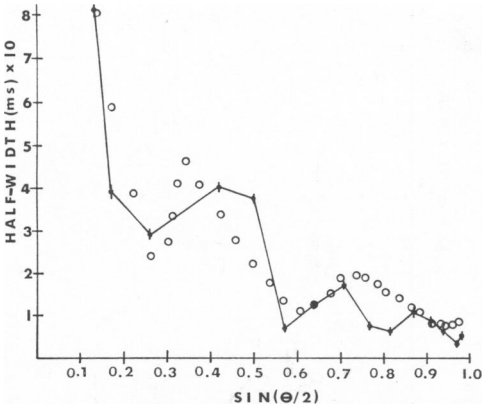

FIGURE 8 Scaling curve for the data from immotile cells (●) and points calculated with Eq. 16 (○) for the standard shaped particle with a coat of thickness 0.27 μm and an index of refraction of 1.42. The interior index of refraction is 1.35.

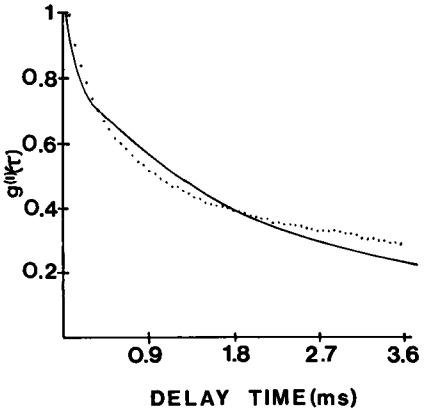

FIGURE 10 Experimental autocorrelation function from a immotile sample at a scattering angle of 80° (···) and a fit generated with Eq. 16 (—) for the standard uncoated particle. All other parameters are the same as those used to fit the data at 15° as shown in Fig. 5.

approximate thickness of the acrosome. The addition of this thick coat leads to an increase in the height of the first peak, but also to a smearing out of the peaks at higher **k**. The problem with a thick coat in our model is that it covers the whole particle and not simply the anterior portion, as in the real spermatozoon. This can, however, be partially overcome by choosing a compromise coat of thickness 0.15 μm, with indices as before, on a particle of size 9.0 × 2.3 × 0.5 μm. This is shown in Fig. 9. The features at high **k** appear, but the lowest peak is shifted too far to agree with the data. As will be mentioned later, we are presently trying to produce other models which may better represent the real system.

There is reasonable agreement between the shapes of the calculated and experimentally determined autocorrelation functions over all scattering angles studied. For example, Fig. 10 shows a model function for the uncoated particle of size 9.0 × 2.3 × 0.5 μm and an experimental autocorrelation function at a scattering angle of 80°. Although there were some weaknesses as indicated earlier, we were generally quite pleased at the overall agreement between the predictions of the model and the data. For this reason we began a similar scaling study of the motile populations of spermatozoa.

Normally Swimming Spermatozoa

The scaling properties of scattering functions from normal cells (Eq. 1) will now be examined. The initial plot (Fig. 11) is one of the data from normally swimming spermatozoa, where the vertical bars again indicate the standard error of the mean of the average value given at that scattering angle, and a curve calculated by means of Eq. 1

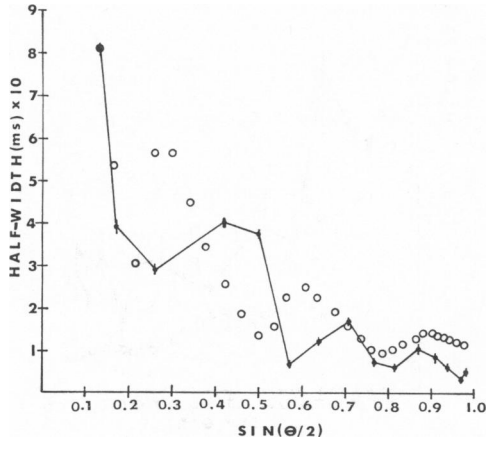

FIGURE 9 Scaling curve for the data from immotile cells (●) and points calculated with Eq. 16 (○) for the standard shaped particle with a coat of thickness 0.15 μm and an index of refraction of 1.42. The interior index of refraction is 1.35.

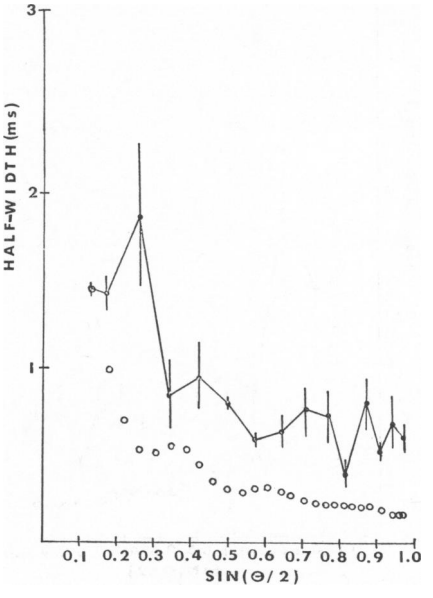

FIGURE 11 Scaling curve for the data from normally swimming spermatozoa (●) and points calculated with Eq. 1 (○) for the standard scatterer without a coat, with the tilt angles as given in the text.

for an uncoated particle having the standard dimensions. In all calculations for the normally swimming sperm, the scatterer is tilted about the b axis by an angle of 57°, and about the a axis by an angle of 12°, so as to imitate the proper trajectory for the cell as given by Craig et al. (1979). As noted by Craig et al. (1979), the rotational frequency of the normal cell was the dominant factor influencing the dynamics of the scattered light. In this plot and all that follow, the data and model were normalized by adjusting the average rotational frequency of the model scatterer until the half-width of its autocorrelation function matched the average of the data at 15°. This frequency was never very different from 10 Hz. The peaks in the model scaling curve have about the same spacing as those of the data but occur at slightly shifted values of $\sin(\theta/2)$. More significantly, the absolute value of the data is always larger than the model.

In this case, changing the thickness of the scatterer, the a parameter, to a value of 0.45 μm, gives the improved agreement shown in Fig. 12. Adjusting b or c by small amounts again had minimal effect. When a thin coat (thickness = 0.01 μm, refractive index = 1.42) was added to the particle of size 9.0 × 2.3 × 0.45 μm, there was no improvement in the scaling behavior. As in the immotile case, however, the scaling may be improved by adding a thick coat to model the acrosomal region. This is shown in Fig. 13, where a particle of size 9.0 × 2.3 × 0.5 μm is modeled with a thick coat (0.27 μm) and indices as before. In the high **k** region, the features are again smeared out owing to the dominance of the coat in the scattering process. The compromise thickness of 0.15 μm yields the scaling curve shown in Fig. 14. There is now relatively good agreement at $\sin(\theta/2) \sim 0.26$, but again the peaks at high **k** are smeared out.

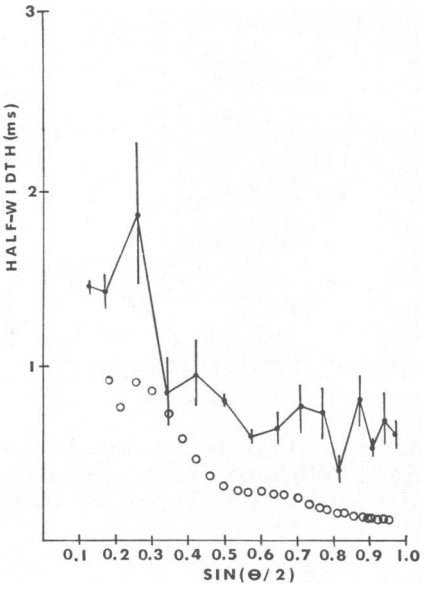

FIGURE 13 Scaling curve for the data from normally swimming spermatozoa (●) and points calculated with Eq. 1 (○) for the standard scatterer with a coat of thickness 0.27 μm with an index of refraction of 1.42. The interior index of refraction is 1.35.

There still remains a significant difference in the absolute value of the data and the theory, especially at higher **k**. The one parameter that significantly influenced the magnitude of the scaling curve was length of the c axis. If the value of c is made smaller at higher **k**, one can achieve good agreement. Physically this might indicate that one is

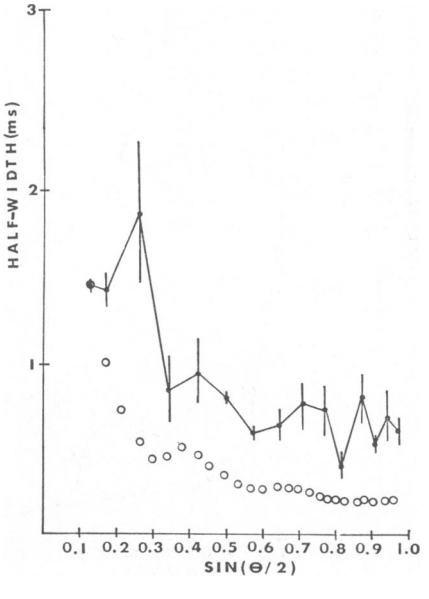

FIGURE 12 Scaling curve for the data from normally swimming spermatozoa (●) and points calculated with Eq. 1 (○) for an uncoated scatterer of semiaxes 9.0 μm × 2.3 μm × 0.45 μm.

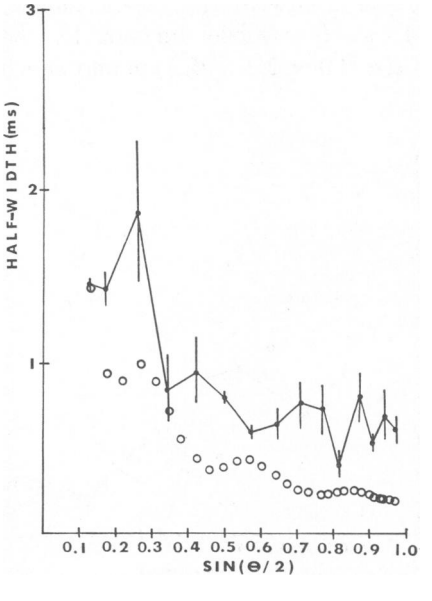

FIGURE 14 Scaling curve for the data from normally swimming spermatozoa (●) and points calculated with Eq. 1 (○) for the standard scatterer with a coat of thickness 0.15 μm with indices of refraction as stated earlier.

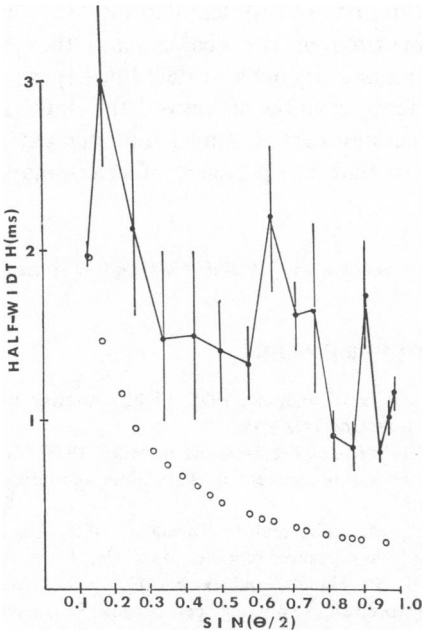

FIGURE 15 Scaling curve for the data from defectively swimming spermatozoa (●) and points calculated with Eq. 7 (○) for a particle of semiaxes 9.0 μm × 2.3 μm × 0.45 μm with a coat of thickness 0.01 μm and indices of refraction as stated earlier. γ_0 has a value of 50° and R_0 a value of 6.8 μm. All other parameters are given in the text.

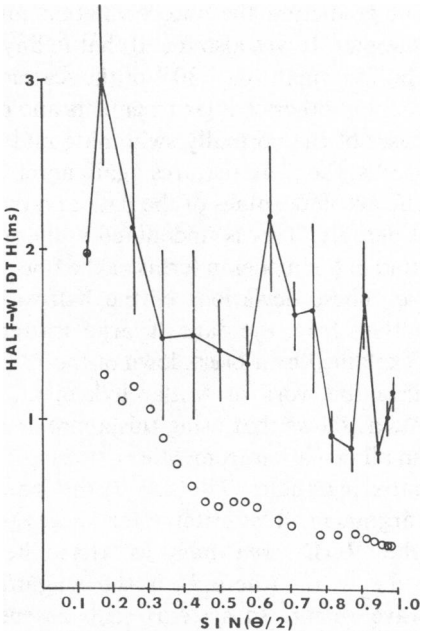

FIGURE 16 Scaling curve for the data from defectively swimming spermatozoa (●) and points calculated with Eq. 7 (○) for a particle of semiaxes 9.0 μm × 2.3 μm × 0.45 μm with a coat of thickness 0.15 μm with indices of refraction as stated earlier. γ_0 has a value of 72° and R_0 a value of 2.8 μm. All other parameters are given in the text.

probing smaller internal structures at higher **k**. This possibility is, of course, not included in our present model. The effects of c did not occur in scaling curves of the immotile cells since $\mathbf{k} \cdot \mathbf{c} = 0$ for that case.

Defectively Swimming Cells

A coat was found to be an integral part of the model used to fit the autocorrelation functions from defective cells at a scattering angle of 15° (Craig et al., 1982) and is included in all scaling curves shown here. The particle is again modeled as an ellipsoid of dimensions 9.0 × 2.3 × 0.45 μm. According to the cinematographic data (Craig et al., 1982), the maximum in-plane tilt angle of the head (β_0) will be taken to be 50°. The average speed and frequency of the scatterers will be chosen to be 93 μm/s and 14 Hz, with standard deviations (σ_v and σ_f) 42.3 μm/s and 8.5 Hz, respectively. Variations of R_0 and γ_0 will be considered below.

Fig. 15 shows the scaling data from defectively swimming cells as well as a model scaling curve calculated with Eq. 7. Again, the vertical bars on the data indicate the standard error of the mean. The magnitude of the tilt angle, γ_0, was very difficult to obtain from the cinematography, although measurements indicated that 50° was the minimum value it could be. R_0, however, was found, fairly accurately, to be 2.8 ± 0.50 μm. The calculated scaling curve in Fig. 15 was determined for $\gamma_0 = 50°$. This required a value of R_0 that was unreasonably high at 6.8 μm, but it was included to show the lack of features in the model. This lack of feature is probably due to a cancellation effect between the in-plane and the out-of-plane motion.

As in the normal and immotile cases, the best scaling behavior was seen for the compromise coat thickness of 0.15 μm (refractive index, 1.42). This is shown in Fig. 16. A value for γ_0 of 72° was required to match the half-width at 15°. The peaks are present in this model and in rough agreement with the data.

The absolute values of the experimental and the calculated scaling curves remain in significant disagreement, as in the case of the normal cells. Again, however, the disagreement at higher scattering angles could be removed if lower values of c were chosen. This implies that the present model lacks sufficient internal or small-scale structure.

CONCLUSIONS

In this work, spermatozoa were best modeled as coated RGD ellipsoids of size 9.0 × 2.3 × 0.45 μm. The scaling curves calculated for this system exhibit some of the same properties as data from normally swimming, defectively swimming, and immotile spermatozoa, but significant differences as well.

For immotile cells, the model and experimental results agree very well both in terms of the positions of the features present in the scaling curves as well as the absolute values. This shows that the combination of a sinking rotating ellipsoid plus a diffusing particle model

does well at predicting the autocorrelation functions for immotile samples. It was also found that in any particular sample of bull spermatozoa ~30% of the scatterers are not spermatozoa, but other cellular fragments and debris.

In the cases of the normally swimming and defectively swimming cells, the peak features again agree fairly well, although the absolute values of the data and model curves differ considerably. This is undoubtedly due to a lack of sophistication in the model in terms of the fine structure of the particle. These deviations of the half-widths of the model functions from the data at large scattering angles cannot be explained by a breakdown of the RGD approximation, since the work of Kotlarchyk et al. (1979) on similar systems shows that using this approximation leads to only a small deviation from Mie scattering results even at large scattering angles. This can be rationalized by the following argument. The criteria for successful application of the RGD treatment is that the quantity $k_0 d|(m - 1)| \ll 1$, where k_0 is the magnitude of the incident wave vector. In systems such as spermatozoa, where the refractive index of the interior (1.35) nearly matches that of the solution (1.33), the bulk of the scattering arises at the outer surface. Hence, one observes the large effects of a coat ($n = 1.42$), which were noted earlier. For such a system, the appropriate thickness d is the coat thickness (~0.15 μm). Hence, the criteria evaluate to ~0.1 and the requirement is clearly satisfied.

In all cases, it was necessary to add a thick coat (~0.15 μm) to the ellipsoid to achieve best agreement. We conclude from this that the acrosome, a thick cap on the anterior region of the cell, contributes significantly to the scattered field.

The treatment used in this work required that the thick coat extend completely over the whole surface of the ellipsoid. In the case of motile cells, this approach allows meaningful interpretation of autocorrelation functions obtained at low scattering angle where coat effects are small. Models which can be applied successfully over the whole range of scattering angles will require somewhat more detail. Such a model would require a thick coat on the anterior part of the ellipsoid tapering to a thin coat on the back region. Models that do this complicate the calculations further but are presently being investigated.

The results presented here are in disagreement with those of Shimizu and Matsumoto (1977), who found for the spermatozoa of the abalone and the pig that the autocorrelation functions scaled linearly as $1/k$. They found no features in the curves of half-width vs. scattering angle. The number of angles investigated was small, however, so that the presence of peaks may have been missed.

Received for publication 4 March 1981 and in revised form 8 July 1981.

REFERENCES

Asano, S., and G. Yamamoto. 1975. Light scattering by a spheroidal particle. *Appl. Opt.* 14:29–49.

Ascoli, C., M. Barbi, C. Frediani, and A. Muré. 1978. Measurements of *Euglena* motion parameters by laser light scattering. *Biophys. J.* 24:585–599.

Chen, S.-H., M. Holz, and P. Tartaglia. 1977. Quasi-elastic light scattering from structured particles. *Appl. Opt.* 16:187–194.

Craig, T., F. R. Hallett, and B. Nickel. 1979. Quasi-elastic light scattering spectra of swimming spermatozoa. Rotational and translational effects. *Biophys. J.* 28:457–472.

Craig, T., F. R. Hallett, and B. Nickel. 1982. Motility analysis of circularly swimming bull spermatozoa by quasi-elastic light scattering and cinematography. *Biophys. J.* 38:63–70.

Fawcett, D. W., and J. M. Bedford, editors. 1979. The Spermatozoon: Maturation, Motility, Surface Properties, and Comparative Aspects. Urban & Schwarzenberg, Inc., Baltimore, MD.

Hallett, F. R., T. Craig, and J. Marsh. 1978. Swimming speed distributions of bull spermatozoa as determined by quasi-elastic light scattering. *Biophys. J.* 24:203–216.

Holz, M., and S.-H. Chen. 1978*a*. Structural effects in quasi-elastic light scattering from motile bacteria of *E. coli*. *Appl. Opt.* 17:1930–1937.

Holz, M., and S.-H. Chen. 1978*b*. Rotational-translational models for interpretation of quasi-elastic light scattering spectra of motile bacteria. *Appl. Opt.* 17:3197–3204.

Kotlarchyk, M., S.-H Chen, and S. Asano. 1979. Accuracy of RGD approximation for computing light scattering properties of diffusing and motile bacteria. *Appl. Opt.* 18:2470–2479.

Racey, T. J., F. R. Hallett, and B. Nickel. 1981. A quasi-elastic light scattering and cinematographic investigation of motile *Chlamydomonas reinhardtii*. *Biophys. J.* 35:557–571.

Rikmenspoel, R. 1964. Electronic analyzer for measuring velocities and concentration of spermatozoa. *Rev. Sci. Instrum.* 35:52–57.

Shimizu, H. and G. Matsumoto. 1977. Light scattering on motile spermatozoa. *I.E.E.E. (Inst. Electr. Electron. Eng.) Trans. Biomed. Eng.* 24:153–157.

van Duijn, Jr. C., and C. van Voorst. 1971. Precision measurements of dimensions, refractive index, and mass of bull spermatozoa in the living state. *Mikroskopie.* 27:142–167.